
Universidad Zaragoza


Master's Thesis

# Electric control of spin qubits

Author:

SEBASTIÁN ROCA JERAT

Supervisors:

DAVID ZUECO LÁINEZ
FERNANDO LUIS VITALLA

Department of Condensed Matter Physics
Faculty of Science
University of Zaragoza

"*La esperanza, la que de veras vale la pena, es la que desayuna dudas cada mañana.*"

*Eduardo Galeano*

Muchas gracias a todas las personas que me han acompañado a lo largo de este año tanto dentro como fuera de la universidad, su ayuda y apoyo siempré serán el mejor regalo.

Agradecer también al Instituto de Nanociencia y Materiales de Aragón (INMA-CSIC) por su programa PI2, dentro del cual se ha desarrollado este trabajo.

# Contents

# Introduction

The potential of a quantum computer lies in the nature of its main constituents, the qubits, which open completely novel ways to process information and give access to non-classical information states. The difference with classical bits is the possibility of not only having $|0\rangle$ or $|1\rangle$ states but also any superposition of them. Besides, two qubits can be entangled so that measurements on one of them affect the other without the need to operate explicitly on it, which cannot be emulated in classical computers.

To have a functional quantum computer one has to be able to manipulate each of the qubits individually and to perform conditional operations between any two of them. These two properties confer universality to a computer. In order to achieve it, the qubits must be controlled and wired together through (superconducting) circuits. This unravels one problem: decoherence. Any quantum system that is not totally isolated from its environment interacts with a large number of degrees of freedom (environment) causing dissipation and decoherence. The first one takes place in the characteristic time $T_1$ of relaxation towards thermal equilibrium. Dephasing, on the other hand is more subtle and it has no classical analogue. In this process there is a loss of coherence between states $|0\rangle$ and $|1\rangle$, turning quantum superpositions into a classical mixed state of 0's and 1' s. The time at which this occurs is denoted as $T_2$.

Macroscopic qubits based on solid-state circuits have already been implemented and assembled into the first small scale quantum processors (also known as NISQs for "Noisy Intermediate Scale Quantum systems") [1–3]. However, being macroscopic, they present problems for scaling-up to a sufficiently high computational power. In order to integrate more qubits in each device, microscopic systems, such as nuclear spins, trapped atoms or ions or impurity spins in solids, provide a quite obvious choice. However, these systems are very difficult to wire up and almost impossible to tune, i.e. to modify their properties. An intermediate solution between these natural systems and circuits lies in artificial magnetic molecules. [4]. Molecules are the smallest object that remains tuneable yet fully reproducible by nature. Besides, it is also possible to have more than two operational levels, such that the molecule acts as a qudit [5]. This allows integrating non-trivial quantum functionalities, even simple algorithms, in a well-defined microscopic object.

Another advantage of magnetic molecules is that they can be controlled and wired through photons in superconducting circuits on an experimentally accessible scale [6]. However, there are challenges here. The most intuitive way to couple to a spin is through magnetic fields. On the one hand, since a current is needed to generate them, these methods are energy-consuming. On the other hand, if they are generated in superconducting materials, their critical current places a limit to the maximum attainable spin-photon coupling and makes it difficult to confine it spatially. An attractive solution to these drawbacks is to use the electric field for this task. However, this is also a challenge since, in principle, the spin cannot be directly coupled to the electric field.

This is the problem we are going to address in this master's thesis. First, in section 1, we study the mechanisms by which a molecule can be affected by an electric field and what kind of phenomenology we can find. Then, in section 2, we describe a material candidate that could present a suitable magnetoelectric coupling. Finally, in section 3, with all the information acquired, we study the coupling between light and matter and present designs of superconducting circuits with which we could experimentally observe this coupling.

# 1 Electric field sensitivity of molecular spin qubits

## 1.1 Ion's environment: Crystal Field

When studying the properties of a certain ion, the interactions of its valence electrons with the surroundings must be taken into account. This is the case of magnetic molecules, formed by individual 3d ions. Let us discuss the effect of these interactions in the spin Hamiltonian.

In a multi-electron ion there are Coulomb-type interactions between each electron and all the external charges. For a 4f ion, the unpaired electrons that define the spin ground state are shielded by the 5s and 5p shells and can therefore be little affected by an external electrostatic potential. However, in a 3d ion, the unpaired electrons are in the outermost shell and will therefore be strongly affected by the potential. In addition, the charge distributions of neighbouring ions can overlap with the charge distributions of our problem ion, which complicates the problem and gives rise to what is known as ligand field theory [7], where the ligands are the charge distributions of the neighbouring ions.

When the effect of the neighbouring ions can be described by a set of point-like charges, the problem can be approached from crystal field theory [8–10]. This theory was developed in the 1930s, when Van Vleck and Bethe described quantitatively the behaviour of paramagnetic ions through an electrostatic potential describing all these interactions with the ion's surroundings.

One of the first consequences of the crystal field is the quenching of the orbital momentum. The crystal field can partially or completely lift the level degeneracy that exists in a free ion. The electronic wave functions adapt to the interaction with its surrounding ions, eventually cancelling all components of the angular momentum. When this happens, the orbital angular momentum ceases to contribute to the magnetic momentum, as found for 3d salts. In other words, the effect of the environment on the ion has large consequences on its magnetic properties. Depending of the strength of this cristal field, there are three different scenarios. When the total angular momentum is a good quantum number (weak field) or not (intermediate field), or whether the field is so strong that it overcomes the spin-orbit interaction (strong field). In general, the potential describing the crystal field has to respond to the symmetries of the crystal itself. In the spin Hamiltonian, which correctly captures the same symmetries, yield the terms like:

$$\mathcal{H}_{\text{cf}} = \sum_{n,m} B_n^m \hat{O}_n^m \tag{1}$$

where $B_n^m$ are material-dependent parameters that can be characterised by EPR and $\hat{O}$ are the Stevens operators, given as powers of spin operators indicated by $n$ (see below) [10]. The index $m$ marks whether these operators have terms only on the diagonal ($m = 0$) or also off the diagonal ($m \neq 0$). The symmetries of the problem restrict the number and type of operators appearing. For example, $n$ odd terms do not appear as they do not preserve the time reversal symmetry. Finally, operators with $n > 2S$ do not appear, provided that $S$ is a good quantum number, we will not have transitions between levels with different $S$. In general, only the lowest order operators are necessary, namely

$$\mathcal{H} = B_2^0 \hat{O}_2^0 + B_2^2 \hat{O}_2^2 \, . \tag{2}$$

The corresponding Stevens operators are related to spin operators as $\hat{O}_2^0 = 3S_z^2 - S(S+1)$ and $\hat{O}_2^2 = \frac{1}{2}(S_+^2 + S_-^2)$. Then, the Hamiltonian can be rewritten in terms of a anisotropy tensor $\tilde{D}$ as

$$\mathcal{H} = \mathbf{S} \cdot \tilde{D} \cdot \mathbf{S} = D_x S_x^2 + D_y S_y^2 + D_z S_z^2 \, . \tag{3}$$

$\tilde{D}$ tensor is traceless ($D_x + D_y + D_z = 0$). Further manipulations are

$$D_x S_x^2 + D_y S_y^2 + D_z S_z^2 = \frac{1}{2}(D_x + D_y)(S_x^2 + S_y^2) + \frac{1}{2}(D_x - D_y)(S_x^2 - S_y^2) + D_z S_z^2 \,, \tag{4}$$

allowing to define the parameters $D \equiv \frac{3}{2} D_z = 3B_2^0$ and $E \equiv \frac{1}{2}(D_x - D_y) = B_2^2$. Ignoring energy shifts that do not affect the difference between levels we finally arrive to

$$\mathcal{H}_{\mathrm{ZFS}} = D S_z^2 + E(S_x^2 - S_y^2) \tag{5}$$

If the system is uniaxial, $D_x = D_y$ and $E = 0$, while $E \neq 0$ whenever there is an orthorhombic distortion.

Let us make an important remark. In EPR experiments, the magnitude of these parameters can be obtained, but not its sign. Consider for example a system with $S = 1$ in the presence of an external magnetic field applied along the direction denoted as $z$:

$$\mathcal{H} = \mathcal{H}_{\mathrm{ZFS}} + g\mu_{\mathrm{B}} B_z S_z \tag{6}$$

In Fig.(1) we plot the spectrum as a function of the external magnetic field. The sign of $D$ determines the ground state of the system.

At small enough fields, if $D$ is positive the ground state is $M = 0$, while if $D$ is negative the two lowest levels are given by the doublet $M = \pm 1$. As a first consequence, only in the former case transitions between the fundamental and the first excited can be performed with an external field since $\Delta M = \pm 1$.

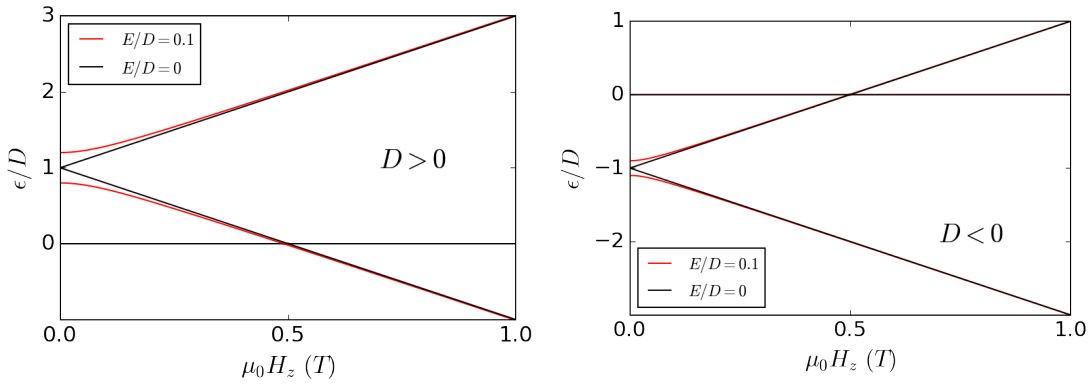


(a) (b)

Figure 1: Schematic of levels of Eq.(6) for different values of the Hamiltonian parameters. In (a) is represented the situation with $D > 0$ in which the fundamental state corresponds to the state $M_s = 0$. The separation between this and the other two zero-field states corresponds to precisely the value of $D$. The parameter $E$ lifts the remaining degeneracy between the $M_s = \pm 1$ states. In (b) we have the same representation but for the case $D < 0$, where here the ground state is formed by the $M_s = \pm 1$ doublet.

## 1.2 Electrical coupling

If the ion's magnetic properties are modified by the presence of adjacent charge distributions, an external electric field can perturb such distributions and, thereby, modify the ion magnetic

properties. The effect of the interaction between an electric field and an ion leads to the Stark effect, in which the spectral lines are modified by the electric field through the operator [10]:

$$\mathcal{H}_{\text{Stark}} = -(-e)\mathbf{E} \cdot \sum_p \mathbf{r}_p = -\mathbf{E} \cdot \mathbf{p}_e \tag{7}$$

where $\mathbf{p}_e = -e\sum_p \mathbf{r}_p$ is the electric dipole operator of the ion and $\sum_p \mathbf{r}_p$ sums over the positions of the electrons surrounding it. If the electric fields are smaller than the interactions between the ion and the environment and restricting ourselves to the lowest energy levels, we can use perturbation theory. First order effects induce changes proportional to the field,

$$\Delta_1 W_E = -\mathbf{E} \cdot \langle \mathbf{p}_e \rangle \tag{8}$$

where $\langle \mathbf{p}_e \rangle$ is taken over the ground state or ground manifold (if there is a degeneracy). Higher order effects, known as polarization effects, usually depend quadratically on electric field. For instance, second-order terms are

$$\Delta_2 W_E = \sum_{n\neq 0} \frac{\langle 0| \mathbf{E} \cdot \mathbf{p}_e |n\rangle \langle n| \mathbf{E} \cdot \mathbf{p}_e |0\rangle}{E_0 - E_n} \tag{9}$$

Electric fields obtained in the laboratory are much more smaller than the electric fields generated by the ion charges. For example, consider a 220 V voltage source applying an electric field in a region of 1 centimetre (e.g. between two parallel plates). The field generated is $2.2 \times 10^4$ V/m. On the other hand, the electric field generated by an elementary charge at a distance equal to the Bohr radius, is $5.142 \times 10^{11}$ V/m, i.e. 7 orders of magnitude higher. Therefore $\langle 0| \mathbf{p}_e \cdot \mathbf{E} |n\rangle$ is much more smaller than the energy differences of the Stark operator, $E_0 - E_n$. Thus, the first order effect is dominant, provided it is not suppressed by selection rules.

These selection rules are mainly imposed by the crystal symmetries, in particular inversion symmetry. If the Hamiltonian has inversion symmetry, the ground state of the system will be either even or odd, and therefore the expected value of the dipole moment will cancel because it is an odd function (changes sign through inversion). On the other hand, if the Hamiltonian lacks such symmetry, the expected value may not be zero. Consider, then, that the system has no centre of inversion so that the crystalline electrostatic potential, $V(r)$, contains an antisymmetric contribution, $V_{odd}$. The first-order perturbation is then:

$$\Delta_1 W_E = -\sum_{n\neq 0} \frac{\langle 0| \mathbf{p} \cdot \mathbf{E} |n\rangle \langle n| V_{\text{odd}} |O\rangle + c.c.}{E_0 - E_n} \tag{10}$$

As described above, the main contributions come from internal crystalline fields so $V_{\text{odd}}$ dominates over the Stark operator and the linear or first order term.

With all this at hand, we search for systems that lack inversion centre. Whether it is because we want to tune any particular resonance, e.g. the level splitting that defines the frequency of a spin qubit, or because we want to coherently control the spin state through AC electric field.

In the literature, there are several examples of magneto-electric coupling through various effects. In general, they all exploit the lack of inversion symmetry. In addition, this effect can be further exploited if there is a strong spin-orbit coupling, so that the orbital modulations induced by the electric field affect the spin. Some works explore the intensity modulation of the exchange interaction in antiferromagnetic systems that are arranged in triangles (no centre

of inversion) [11, 12]. This effect has been observed by means of EPR studies [13] as well as in experiments on Quantum Dots (QDs), demonstrating that spin-orbit interaction enables an electrical coherent control of their spin states [14, 15]. EPR measurements on molecular helices based on Manganese compounds [16] have shown that modulation of the magnetic exchange by electric fields can also occur in this type of structure. In this case, is the interaction between the spin of Manganese and that of the radicals. Thus, there are several options to modulate magnetic exchange interactions through electric fields and to observe these effects experimentally, also in the spin of single electrons in QDs.

In $TbPc_2$ molecules [17], the interaction of external electric fields with the magnetic properties via the hyperfine interaction between the nuclear and the electron spins allows an electric control of nuclear spin states. The authors refer to this effect as the hyperfine Stark effect, which provides yet another possibility to handle qubits electrically.

Finally, the one that we will explore in this work. The modification of the magnetic anisotropy: external electric fields can modify the charge distributions in such a way that they modify the effect of the crystalline field on the ion and, therefore, the magnetic anisotropy [18]. This allows coherent control of single magnetic molecules in materials with high electrical polarizability, as we will see in section 2.

### 1.3 Spin Hamiltonian and selection rules

We are going to consider a uniaxial system with the following generic spin Hamiltonian:

$$\mathcal{H}_{\text{spin}} = \mathcal{H}_{\text{ZFS}} + \mathcal{H}_{\text{Zeeman}} + \mathcal{H}_{\text{Hyp}} \tag{11}$$

We consider orthorhombic symmetry where both parameters ($D_{\parallel}$ and $D_{\perp}$) depend linearly on the electric field. This allows generating a non-zero $D_{\perp}$ even when the crystal does not have such term in the zero electric field scenario and gives another way to control and modify the symmetries of our system.

$$\mathcal{H}_{\text{ZFS}} = \mathcal{H}^{0}_{\text{ZFS}} + \mathcal{H}^{\text{induced}}_{\text{ZFS}} = D^{0}_{\parallel} S_z^2 + D^{0}_{\perp}(S_x^2 - S_y^2) + \kappa_{\parallel} E^{z}_{\text{ext}} S_z^2 + \kappa_{\perp}(E^{x}_{\text{ext}} S_x^2 - E^{y}_{\text{ext}} S_y^2) \tag{12}$$

We consider that the $g$-tensor having the same principal axis as the $\tilde{D}$ tensor. Finally, we consider an isotropic nuclear spin. In any case, the nuclear Zeeman interaction it is neither the dominant effect nor the main interest in our discussion.

$$\mathcal{H}_{\text{Zeeman}} = \mu_{\text{B}} \vec{B}_{\text{ext}} \cdot \tilde{g} \cdot \vec{S} - g_{\text{N}} \mu_{\text{N}} \vec{B}_{\text{ext}} \cdot \vec{I} \tag{13}$$

Finally, the nuclear and electronic spins are coupled via the hyperfine interaction. We then introduce a hyperfine coupling tensor $A$, whose principal axes are the same as the other ones.

$$\mathcal{H}_{\text{Hyp}} = A_{\parallel} S_z I_z + A_{\perp}(S_x I_x + S_y I_y) \tag{14}$$

Equation (12) allows inducing spin transitions through microwave electric field pulses.This might lead to faster operation speeds with respect to those generated with magnetic fields and can facilitate the spatial confinement of the control fields, thereby avoiding cross-talk effects with neighbour spins.

Time dependent perturbation theory gives the transtiton rates. If they are described by sine/cosine oscillatory functions the transition probability between two levels, labelled as $i$ and

$j$, is given by:

$$\mathcal{P}_{if}(t;\omega) = \frac{|W_{if}|^2}{4\hbar}\left|\frac{1-e^{i(\omega_{if}+\omega)t}}{\omega_{if}+\omega} + \frac{1-e^{i(\omega_{if}-\omega)t}}{\omega_{if}-\omega}\right|^2 \tag{15}$$

with

$$W_{if} = \langle i|\, W\, |f\rangle \ . \tag{16}$$

Here, $W$ is the corresponding operator that drives the transition. Considering spin transitions and that the microwave radiation will contain now both magnetic and electric fields, labeled as $\vec{b}_{\rm rf}$ and $\vec{e}_{\rm rf}$, respectively. In each case, $W$ is given in Eq.(12) and Eq.(13) Therefore the magnetic tranisitons is modulated by

$$p_{\rm m} = \mu_B|\langle i|\, g_{\parallel}b^z_{\rm rf}S_z + g_{\perp}(b^x_{\rm rf}S_x + b^y_{\rm rf}S_y)\,|j\rangle\,| \tag{17}$$

while the electric induced transitions by

$$p_{\rm e} = |\langle i|\, \kappa_{\parallel}e^z_{\rm rf}S^2_z + \kappa_{\perp}(e^x_{\rm rf}S^2_x - e^y_{\rm rf}S^2_y)\,|j\rangle\,| \tag{18}$$

The transition probability between two levels will be greater the stronger the coupling is.

Let us compare both electrical and magnetic induce transitions. First, the coupling magnitude: while $g\mu_B$ has a value of about 28 GHz/T, of $\kappa$ reported for different materials are around 10 Hz/ $\mathrm{Vm}^{-1}$[18]. It should also be noted that, for a single photon confined in on-chip resonators, the magnetic field amplitude is of order 1 nT whereas the electric field amplitude is of order 0.1 V/m. Thus, ($g\mu_{\rm B}b_{\rm rf} \approx 28$ Hz vs $\kappa e_{\rm rf} \approx 1$ Hz), can be comparable. Finally, while the magnetic transition is mediated by the operator $S_x \propto S_+$ with $\langle m'|\, S_+\, |m\rangle = \delta_{m',m+1}\sqrt{S(S+1)-m'm}$, the electrical transition is mediated by $S^2_x$. Concretely, if in Eq.(18) the $x$ and $y$ components of the rf field are equal, $p_{\rm e} \propto (S^2_+ + S^2_-)$. That is, magnetic transitions connect levels differing $|\Delta m|= 1$ while the electric ones lead to a different $|\Delta m|= 2$ selection rule. Considering a spin with $S = 5/2$ and $D > 0$ (the ground state will be the $m = \pm 1/2$), the relevant matrix elements for transitions from the ground state are $\langle 1/2|\, S_+\, |-1/2\rangle = 3$ for the magnetic case and $\langle 3/2|\, S^2_+\, |-1/2\rangle = 3\sqrt{8}$ for the electric one. From this brief discussion we can conclude that, in principle, the electric coupling is not as small as it might a priori.

A final interesting case is that of an uniaxial system with $\kappa_\perp = 0$. Since the spin Hamiltonian in this situation is $\mathcal{H} = DS^2_z$ (let us exclude the hyperfine interaction for simplicity in this example) it commutes with the operator inducing the transitions (it is the same operator). Therefore electric field mediated transitions are forbidden. A solution is to apply an external perpendicular magnetic field so that the Hamiltonian no longer commutes with $S^2_z$.

# 2 A promising candidate: a manganese center in a piezoelectric "molecular trap"

## 2.1 The sample: Mn(Me$_6$tren)Cl_ClO$_4$

In this master thesis we study a Mn(II) compound, Mn(Me$_6$tren)Cl_ClO$_4$, which does not posses an inversion center and that shows a very high electric polarizability, behaving as a piezoeletric material. This molecule has been synthesised and characterised by Talal Mallah, a collaborator at the University of Paris-Saclay, who provided the data shown in Table 1 (although the nuclear g-factor, $g_{\rm N}$, was extracted from [8]). In this case the parameter $D_\parallel$ comes from the interaction

between the ground state (sextet) with an excited state with different spin value (quadruplet), and in such cases the value tends to be positive. This is something that has been indicated to us by our collaborator but could not be measured directly since, as we have discussed in section 1, from the available EPR data, only the magnitude of this parameter can be obtained, not its sign. The axis that we choose here as quantization axis, the $\hat{z}$ axis, is the magnetic anisotropy C3 axis, depicted in Fig. 2, whereas the external magnetic field will be applied within the $XZ$ plane at an angle $\theta$ with the symmetry axis.

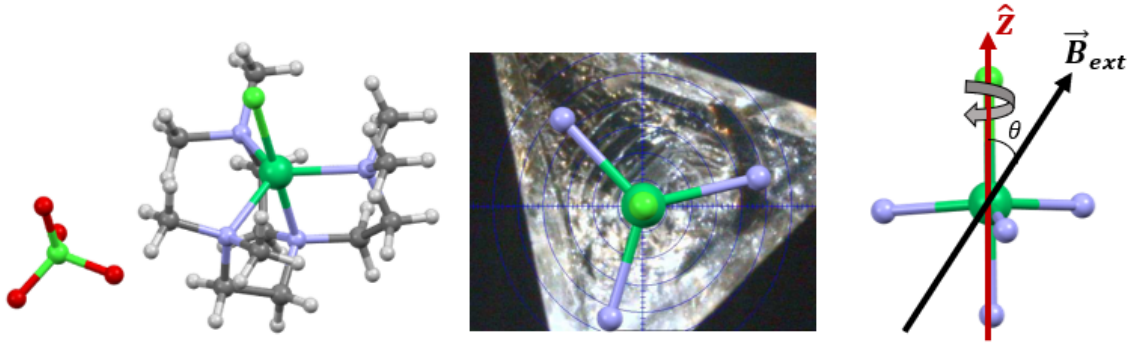


Figure 2: Molecular structure of the target compound synthesised by Talal Mallah of the Universtié Paris-Saclay. On the left is shown the chemical composition as well as the spatial distribution of an individual molecule (the largest central atom corresponds to the Mn(II) ion, the purple ones to Cl, the green ones to N, the red ones to O and the rest to carbons and hydrogens). The central image shows one of the crystals synthesised by our collaborators with the orientation indicated by the superimposed top view of the molecule. On the right is shown the reference system chosen to work with, where $Z$ indicates the uniaxial anisotropy axis and the external magnetic field lies within the $XZ$ plane.

| **Parameter** | S | I | $g_{\parallel}$ | $g_{\perp}$ | $D_{\parallel}$ | $A_{\parallel}$ | $g_{\mathrm{N}}$ |
|---|---|---|---|---|---|---|---|
| **Value** | 5/2 | 5/2 | 2.03 | 2.00 | 4.68 GHz | 186 MHz | 1.3872 |

Table 1: Spin Hamiltonian parameters for Mn($Me_6$tren)Cl_$ClO_4$ provided by our colaborators.

Simulations carried out by the same collaborator give us a first estimate for the electrical coupling parameters of this molecule (see Table 2). These simulations study the effect of homogeneous electric fields on the properties of the magnetic anisotropies considering electric field induced deformations of the crystalline structure (piezoelectric effect). Although these simulations were made on another Cobalt complex, the structure is practically the same as the Mn(II), so it is reasonable to assume that the coupling values will be similar. It should be emphasised that this is not a determination of the coupling but an estimation of the possible couplings that could be achieved. The determination of these parameters will have to be done by spectroscopic techniques.

| $\kappa_{\parallel}$ | $\kappa_{\perp}$ |
|---|---|
| 21.8786 Hz / $\mathrm{Vm}^{-1}$ | 4.6674 Hz / $\mathrm{Vm}^{-1}$ |

Table 2: Values determined for the electric coupling constants for each magnetic anisotropy parameter.

Note that although the crystal does not exhibit rhombic anisotropy, the application of an external electric field along a perpendicular direction respect to the C3 axis breaks this symmetry by introducing a non-zero rhombic term (now $D_{xx} \neq D_{yy}$) through the $\kappa_{\perp}$ parameter. For comparison, the results obtained in [18] show a value of $\kappa_{\parallel}$ of 20.8 rad $\mathrm{s}^{-1}$/V $\mathrm{m}^{-1}$ or 3.31 Hz/V $\mathrm{m}^{-1}$, consequently these estimations predict that the complex $\mathrm{Mn(Me_6tren)Cl\_ClO_4}$ is going to be very sensitive to electric fields and therefore it is a great candidate to explore the magnetoelectric spin control.

## 2.2 Energy spectrum and transitions of interest

With all this at hand the spin Hamiltonian can be written as,

$$\mathcal{H}_{\mathrm{s}} = D_{\parallel}^{0} S_z^2 + \mu_{\mathrm{B}} \vec{B}_{\mathrm{ext}} \cdot \tilde{g} \cdot \vec{S} - g_{\mathrm{N}} \mu_{\mathrm{N}} \vec{B}_{\mathrm{ext}} \cdot \vec{I} + A_{\parallel} S_z I_z + \kappa_{\parallel} E_{\mathrm{ext}}^{z} S_z^2 + \kappa_{\perp} (E_{\mathrm{ext}}^{x} S_x^2 - E_{\mathrm{ext}}^{y} S_y^2) \quad (19)$$

The orientation between $B$ and the axis of the molecule will be as described in Fig. 2, $\vec{B}_{\mathrm{ext}} = B_{\mathrm{ext}} \cdot (\sin\theta \hat{u}_x + \cos\theta \hat{u}_z)$. If the field is parallel to $Z$, we obtain the spectrum of Fig. 3 where we can see that, since $D > 0$, the fundamental state is the subspace corresponding to $|M_s| = 1/2$. Recall that if $D$ were negative, the energy spectrum would be the same but inverted. That is, the state with $|M_s| = 1/2$ would not be the fundamental state but the state with the highest energy, while the state with $|M_s| = 5/2$ would be the ground state. The Zeeman effect splits each electronic and nuclear spin level and the hyperfine interaction separates each doublet, revealing the $(2S+1)(2I+1) = 36$ energy levels without any degeneracy. For each multiplet with the same third spin component, we have 6 lines arising from the hyperfine interaction, between which we do not expect transitions, as these would be given by nuclear magnetic resonance, which is very weak ($\mu_{\mathrm{N}} \ll \mu_{\mathrm{B}}$).

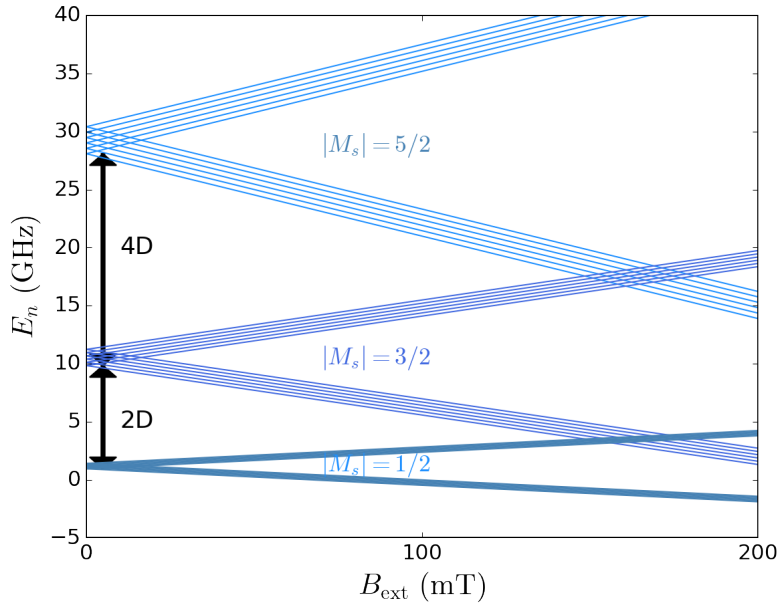


Figure 3: Zeeman and ZFS partially splitting of the energy levels in the case where magnetic field and anisotropy axis are parallel. The ZFS lifts the degeneracy by separating levels associated with different absolute spin projections, while the hyperfine interaction and the electronic and nuclear Zeeman effect lift the remaining degeneracy completely.

It is not always easy to perfectly align the magnetic field with the axis of the molecule or it may not be the most suitable configuration to study certain transitions. As can be seen in Fig. 4, by tilting the magnetic field the spectrum of levels changes radically. Crossings between levels corresponding to the different subspaces become replaced, for $\theta > 0$, by level anticrossings reflecting the mixing of different spin projections induced by transverse magnetic field components. If the energy levels change with the field orientation, so do the transitions between levels: not only the resonance frequencies are shifted by varying $\theta$, but also whether a transition is allowed or not depends strongly on the magnetic field orientation. It is interesting to note that while the levels corresponding to the subspaces of $|M_s|= 3/2$ and $|M_s|= 5/2$ become narrower as $\theta$ increases, the levels of $|M_s|= 1/2$ become wider.

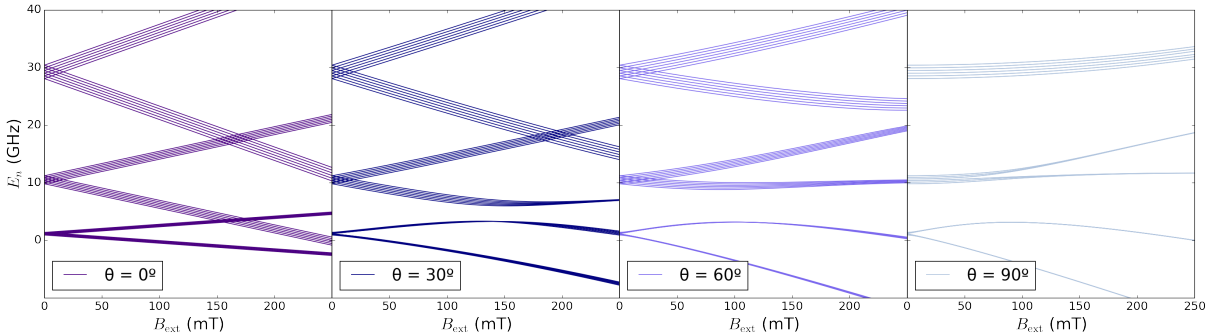


Figure 4: Dependence of the magnetic energy levels on $B_{\text{ext}}$ for different magnetic field orientations with respect to the anisotropy axis. The larger the angle between the two, the smaller the splitting generated by the hyperfine interaction and the greater the mixing of states with different spin projections.

Again, the electric field applied direction is crucial, since the magnetic anisotropies are asymmetrically modified [cf. Eq.(19) and Table 2]. The electric field component parallel to the symmetry axis $Z$ affects more the energy levels that have higher spin projections since the associated operator is $S_z^2$. On the other hand, electric fields perpendicular to the symmetry axis introduces additional mixing into the wave functions of the energy eigenstates. Thus, if we look at Fig. 5, we realise that in the case where the electric field is applied along the $Z$-direction, the levels corresponding to $|M_s|= 5/2$ are modified before those corresponding to $|M_s|= 3/2$, and these in turn before those corresponding to $|M_s|= 1/2$. If the field is perpendicular to $Z$, almost the opposite happens, although all the multiplets start to change at a similar order of field strength. For this study we have also considered that a magnetic field of 100 mT was applied in different orientations to see both effects. As we had already observed in Fig. 4, the application of a magnetic field off the symmetry axis tends to suppress the hyperfine splitting.

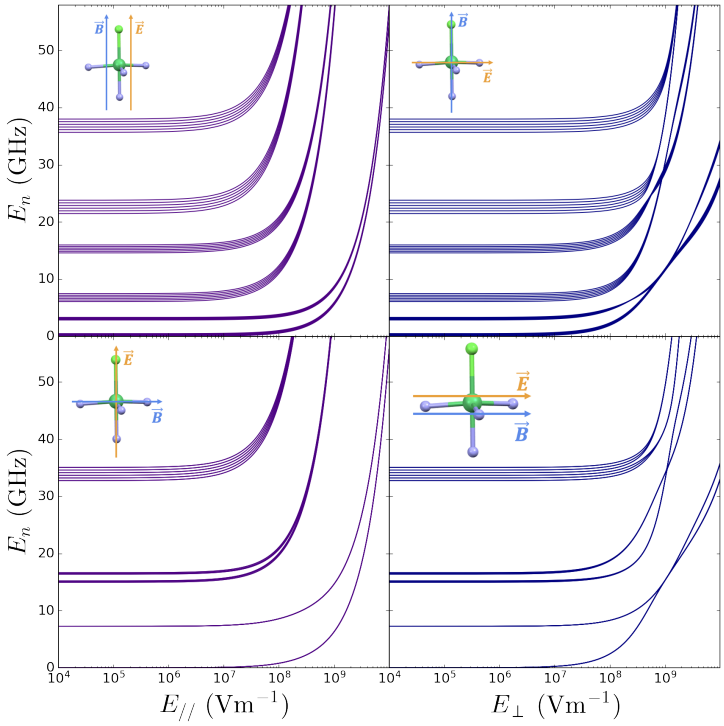


Figure 5: Dependence of energy levels on the applied electric field for different geometries. If we apply a magnetic field (100 mT in the simulations) parallel to the anisotropy axis, the nuclear levels are further apart than if we apply it perpendicularly, while the effect of the electric field is felt earlier if we apply it parallel to the anisotropy axis than if we apply it perpendicularly. In each subplot, the directions of each field with respect to the symmetry axis are indicated by the drawing.

These results confirm the discussion in section 1 that the electric fields that need to be applied to appreciably modify the level scheme are of a gigantic magnitude. Still, they shed light on another type of application. We have mentioned that a 220 V voltage source applied to two plates one centimeter apart from each other generates an electric field which can cause an energy shift of the order of $0.5 - 1$ MHz depending on the spin multiplet and the field orientation. Although this scale is much smaller than the anisotropy energy of the material, it may be sufficient to tune and detune qubits with respect to the frequency of a resonant circuit

having a very narrow resonance. This would be an advantage over tuning qubits with magnetic fields, with which the process is slow and results in large energy dissipation.

However, in this work we are going to focus more on the control through AC electric pulses, so we are now going to study the transitions between levels that would be allowed by the coupling to the electric and magnetic field components of microwave radiation. In what follows, the tuning of the transitions with respect to the frequency of the radiation will be achieved through dc magnetic fields applied along suitable orientations. Let us assume that our $\vec{b}_{\rm rf}$ and $\vec{e}_{\rm rf}$ changes are applied along a generic $\frac{1}{\sqrt{3}}(1,1,1)$ direction with intensities $|\vec{b}_{\rm rf}|=$ 1 nT and $|\vec{e}_{\rm rf}|=0.1$ V/m (the magnitudes of these fields and their spatial distribution will be discussed in section 3). According to Eqs.(17), (18) and taking into account the values in Table 1, we calculate the matrix elements corresponding to the allowed transitions as a function of the orientation of the applied external field (of strength 110 mT for the calculations) and plot them in matrix form in Fig. 6. On the $X$ and $Y$ axes we plot, respectively, the indices corresponding to the initial and final states of each transition. The notation used denotes the 0 state as the ground state, 1 as the first excited state, etc. The colour intensity represents the coupling intensity at that transition, or the Rabi frequency $\Omega_{\rm R}$, in units of Hz per molecule and per photon, since the intensity of the rf fields are normalised to a single photon.

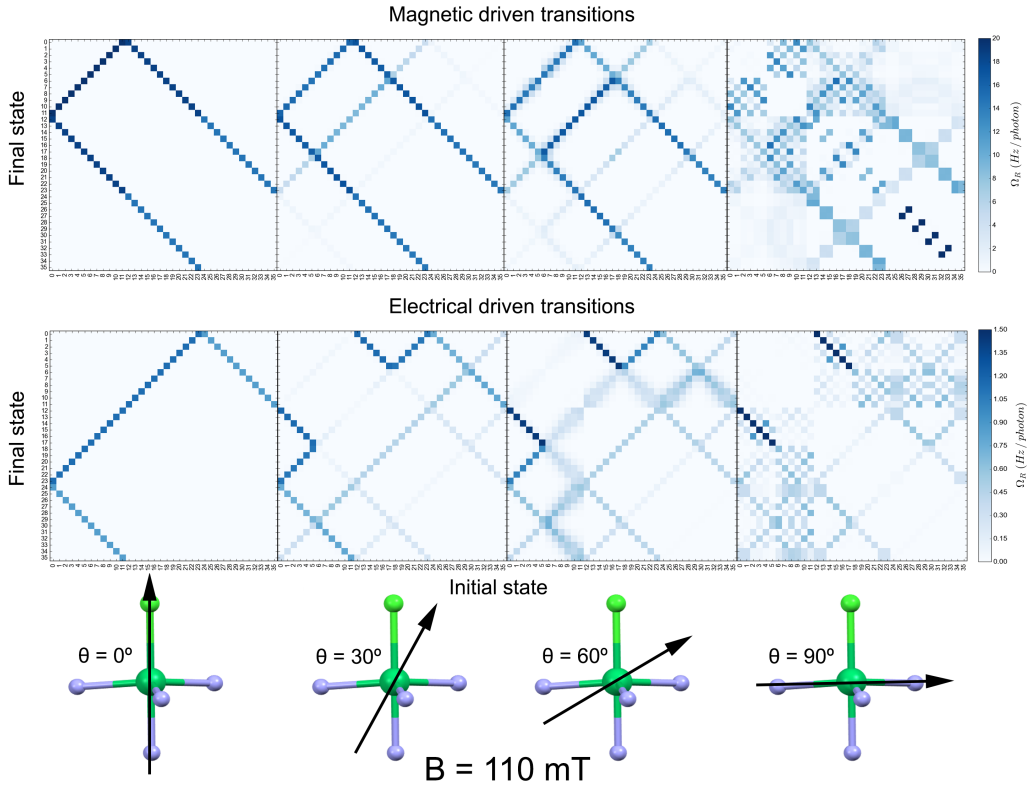


Figure 6: Matrix elements for magnetic and electric driven transitions as a function of the orientation angle between the external DC magnetic field and the symmetry axis of the molecule. The orientation of the microwave fields in charge of inducing the transitions has been chosen completely generically according to a direction vector: $\frac{1}{\sqrt{3}}(1,1,1)$.

If we look at the case of $\theta = 0°$, we see that while the magnetic field couples states

corresponding to $|\Delta m|= 1$, the electric field couples spin projections differing by $|\Delta m|= 2$. As we increase the angle, the overlap between projections increases and progressively more permitted transitions are emerging.

Although the Rabi frequencies obtained in the magnetic case are higher than in the electrical case, it should be noted that this is an estimate to identify which transitions are allowed and what qualitative differences are found between each type of transition in each scenario. The important result here is to note that the matrix elements in both cases are similar and that in principle we can expect coherent control with electric fields for this material.

Since this is precisely our goal, we see now which electric field induced transitions are optimal and under which conditions. We choose the two limiting cases, $\theta = \{0°,\ 90°\}$, for simplicity and we look at Fig. 6 to see which are the matrix elements with the highest value, bearing in mind that the closer the initial state of the transition is to the fundamental level, the better, since we are interested in working at very low temperatures (of the order of 10 mK) to minimise decoherence and, therefore, the excited levels will be sparsely populated, making transitions from these difficult or impossible. Following this criterion, we perform the study presented in Fig. 7. For a parallel orientation between the field and the C3 axis (left figure), we choose the transitions between the ground state and the excited states with indexes 23 and 24 as well as the transition linking states 11 and 12.

$$0 \rightarrow 23 : |S_z = -1/2, I_z = 5/2\rangle \rightarrow |S_z = 3/2, I_z = 5/2\rangle \tag{20}$$

$$0 \rightarrow 24 : |S_z = -1/2, I_z = 5/2\rangle \rightarrow |S_z = -5/2, I_z = 5/2\rangle \tag{21}$$

$$11 \rightarrow 12 : |S_z = 1/2, I_z = 5/2\rangle \rightarrow |S_z = -3/2, I_z = 5/2\rangle \tag{22}$$

As can be seen in the figure, the matrix elements for $0 \rightarrow 23$ and $11 \rightarrow 12$ have the same value, slightly higher than for $0 \rightarrow 24$, and also have lower resonance frequencies. Although we will discuss it later, we are limited in $f_{\text{res}}$ to the frequencies we can work with experimentally (the blue dashed line in the figures marks the maximum attainable frequency). The microwave radiation we can introduce is limited by the design of the circuit and by the readout electronics used and therefore only this range of frequencies has been considered in the discussion. Therefore, it is not only important to maximise the matrix element but also trying to achieve it for the lowest possible resonance frequency, i.e. maximise $p_{\text{e}}/f_{\text{res}}$. According to this criterion, the most favourable transition is $11 \rightarrow 12$ since $f_{\text{res}}$ becomes practically 0 while keeping $p_{\text{e}}$ practically intact. However, when involving the $11^{\text{th}}$ excited state, we can see in the graph below that it has a very low thermal factor, which is expected to severely penalise the transition. On the other hand, the $0 \rightarrow 23$ combines the next to highest $p_{\text{e}}/f_{\text{res}}$ ratio with an ideal thermal factor (involving the G.S.).

If we move to the situation in which the magnetic field is perpendicular to $Z$, (Fig. 7 right), the most important transitions become[1]

$$5 \rightarrow 17 : |S_z = -1/2, I_z = -5/2\rangle \rightarrow |S_z = -3/2, I_z = -5/2\rangle \tag{23}$$

$$6 \rightarrow 18 : |S_z = 1/2, I_z = -5/2\rangle \rightarrow |S_z = 3/2, I_z = -5/2\rangle \tag{24}$$

[1]The labelling of these levels with respect to quantum numbers refers to those in a null-field situation, of course the actual state at an arbitrary field will be a linear combination between different spin projections.

where we see that the dependence on magnetic field is more complex in the inset as a function of the field. The maximum is found at $f_{\text{res}} = 11.248$ GHz and $B_{\text{ext}} = 68$ mT for the transition $5 \rightarrow 17$. This transition also turns out to be the thermally favoured one since it involves the lowest energy multiplet [cf Fig. 3]. The dependence of the matrix elements on magnetic field is no longer trivial as the wave functions become more complex. It should be noted that although we have considered only two transitions, this has been done for the sake of clarity and not to clutter with too much information. There are more transitions that may not be the most ideal or the best matched, but that can also be useful for exploring coherent control. This study is mainly useful to see the resonance frequency of the relevant transitions in order to design the circuits and obtain the necessary experimental conditions, as we will see in the next section.

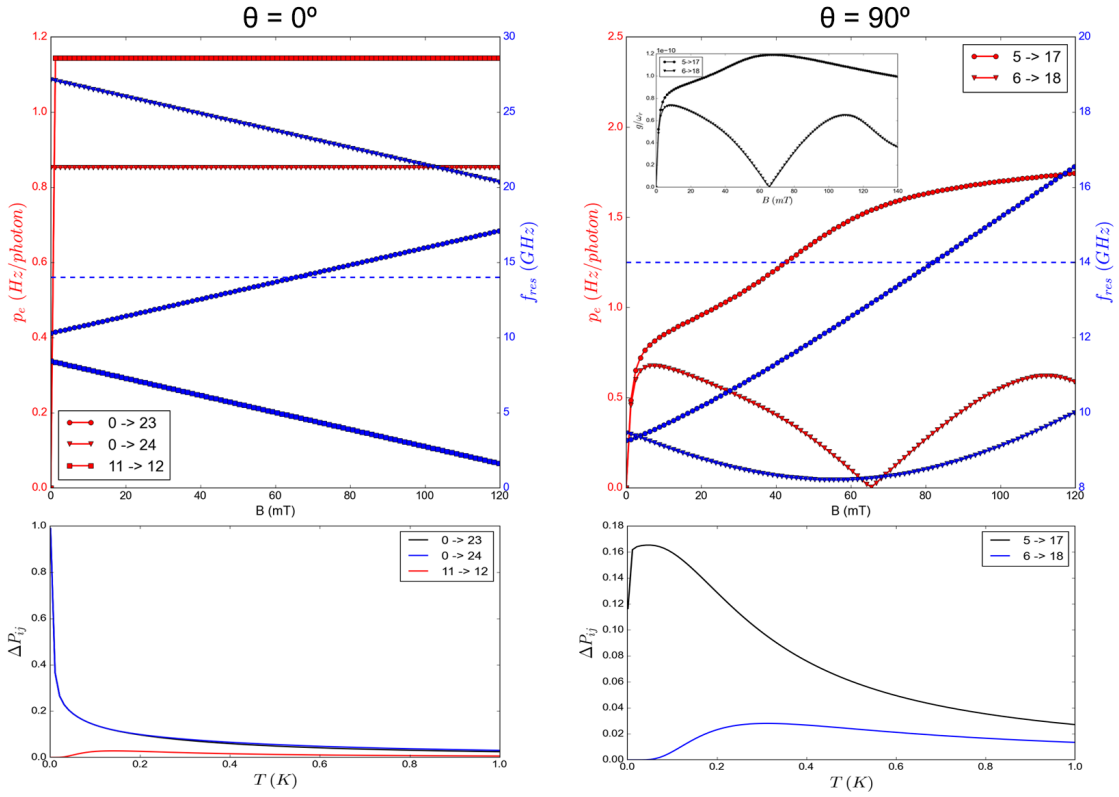


Figure 7: Here is an example of the most relevant electrical transitions in the two extreme cases of the orientation of the external magnetic field versus the crystal symmetry axis. The transitions have been chosen according to the magnitude of their matrix element and their proximity to the ground state. Due to the hyperfine splitting, there are many transitions which are practically equivalent in terms of coupling strength and resonance frequencies. This is a first observation to see the behaviour of what seem to be the most favourable transitions. Red curves show the value of the matrix element for each transition as a function of the magnetic field while blue ones show the resonance frequency for each transition (same legend as for red curves).

## 3 Optimal microwave cavities: LER resonators

When we talk about inducing transitions through AC fields, whether electric or magnetic, we always have to think about what kind of circuit we are going to use to make our sample interact with the radiation. Typically, the samples will be crystals or macroscopic deposits containing

a very large number of molecules. As you might expect, they will not all couple in the same way to the electromagnetic fields unless the fields are perfectly homogeneous. Thus, designing circuits able to generate electric fields of the highest possible strength and homogeneity is crucial to achieve a coherent control of qubits. This scenario where qubits are tuned, controlled and mutually interconnected by electromagnetic circuits or cavities is known as Cavity QED. In our case we are going to work with on-chip superconducting resonators in which we will be able to confine the photons so that they remain oscillating in the circuit for a certain lifetime. In other words, we will be able to describe the radiation trapped in this type of circuit through a bosonic field, or Fock space, where the elementary excitations are the number of photons present in the cavity. Specifically, we are going to work with Lumped Element Resonators (LER).

These are LC resonator circuits coupled to a microwave transmission line through which a readout process is carried out. Each LER is characterised by measuring the dispersion parameter $S_{21} = S_2/S_1$, where indices 1 and 2 refer to the ports at each end of the transmission line. It has a resonant frequency at which the circuit absorbs power from the transmission line and which determines the energy of the photons trapped in it. The quality factor represents the relationship between this resonance frequency and the photon decay rate. The higher the quality factor, the longer the photon remains in the circuit without dissipating and the narrower the resonance peak in the transmission measurement. Specific designs of such circuits optimized to electrically couple to molecular spin qubits will be discussed in section 3.3 while the next two sections discuss the interaction between light and matter in such systems and how to characterise the transmission experiment.

### 3.1 Light-matter coupling

In general, the energy spectrum has more than two levels and with certain resonance frequencies (not necessarily equal) characterizing transitions between each pair of accessible levels (see Fig. 8).

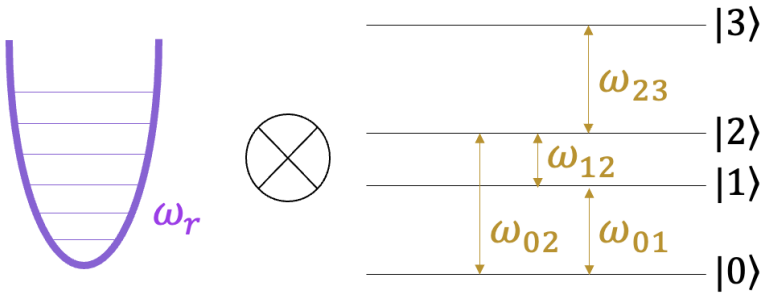


Figure 8: Generic level scheme of a magnetic molecule. For the cavity, we will work in the approximation of a single resonant mode, equivalent to an harmonic oscillator with resonant frequency $\omega_r$

.

Among all these transitions the more relevant is the one that matches the LC resonant frequency $\omega_{ij} \cong \omega_r$ (see Fig. 9). Therefore, we can restrict ourselves to these two states with energy difference $\hbar\omega_{ij}$.


Figure 9: The radiation present in the cavity will only be able to induce transitions if the frequency of the photon, $\omega_{\mathrm{r}}$, matches the resonant frequency of the levels, $\Omega$.

Let $\hat{\mathcal{O}}(\hat{S}, \vec{\xi})$ be the operator inducing such a transition, which can have any dependence on the spin operators, $\hat{S}$, and on the electromagnetic fields $\vec{\xi}$. The interaction Hamiltonian between the resonator and our molecule is then

$$\mathcal{H}_{\mathrm{int}} = \hat{\mathcal{O}}(\hat{S}, \vec{\xi})(\hat{a} + \hat{a}^{\dagger}) \tag{25}$$

where $\hat{a}/\hat{a}^{\dagger}$ are the creation/annihilation operators of the resonator photons (Fock states of the bosonic field).

$\hat{\mathcal{O}}(\hat{S}, \vec{\xi})$ acts on the molecule Hilbert space, projecting it onto the basis generated by the i,j states, $\{|0\rangle, |1\rangle\}$:

$$\hat{\mathcal{O}} = \begin{pmatrix} \langle 0|\hat{\mathcal{O}}|0\rangle & \langle 0|\hat{\mathcal{O}}|1\rangle \\ \langle 1|\hat{\mathcal{O}}|0\rangle & \langle 1|\hat{\mathcal{O}}|1\rangle \end{pmatrix} = \begin{pmatrix} \hat{\mathcal{O}}_{00} & \hat{\mathcal{O}}_{01} \\ \hat{\mathcal{O}}_{10} & \hat{\mathcal{O}}_{11} \end{pmatrix} \tag{26}$$

and defining $\tau^{+} \equiv |1\rangle\langle 0|$, $\tau^{-} \equiv |0\rangle\langle 1|$, $\tau^{z} \equiv \mathcal{I} - 2\tau^{+}\tau^{-}$ we get:

$$\mathcal{H}_{\mathrm{int}} = \left[\hat{\mathcal{O}}_{01}\tau^{-} + \hat{\mathcal{O}}_{10}\tau^{+} + \left(\frac{\hat{\mathcal{O}}_{00} - \hat{\mathcal{O}}_{11}}{2}\right)\tau^{z} + \left(\frac{\hat{\mathcal{O}}_{00} + \hat{\mathcal{O}}_{11}}{2}\right)\mathcal{I}\right](\hat{a} + \hat{a}^{\dagger}) \tag{27}$$

that can be rewritten

$$\mathcal{H}_{\mathrm{int}} = \left[\hat{\mathcal{O}}_{01}\tau^{-} + \hat{\mathcal{O}}_{10}\tau^{+} + (\hat{\mathcal{O}}_{11} - \hat{\mathcal{O}}_{00})\tau^{+}\tau^{-}\right](\hat{a} + \hat{a}^{\dagger}) + \hat{\mathcal{O}}_{00}(\hat{a} + \hat{a}^{\dagger}) \tag{28}$$

We obviate the last term since it is an energy shift and define $\Lambda \equiv \mathcal{O}_{11} - \mathcal{O}_{00}$, $g \equiv \mathcal{O}_{10}$, so that:

$$\mathcal{H}_{\mathrm{int}} = \left[(g\tau^{+} + h.c.) + \Lambda\tau^{+}\tau^{-}\right](\hat{a} + \hat{a}^{\dagger}). \tag{29}$$

This is the Hamiltonian of interaction between a magnetic molecule and the resonator. If we have $N$ molecular spins it is simply given by the sum

$$\mathcal{H}_{\mathrm{int}} = \sum_{i}^{N} \mathcal{H}^{i}_{\mathrm{int}} = \sum_{i}^{N} \left[(g_i\tau_i^{+} + h.c.) + \Lambda_i\tau_i^{+}\tau_i^{-}\right](\hat{a} + \hat{a}^{\dagger}) \tag{30}$$

Let us now discuss the effect of temperature. In general, our $|0\rangle$ state need not be the ground state (see Fig. 10).

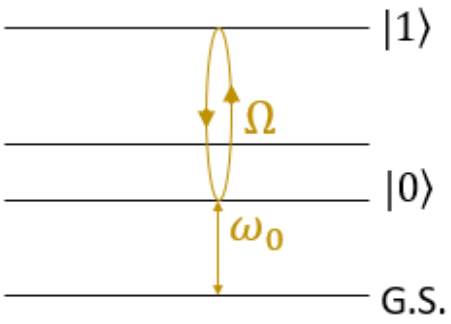


Figure 10: If the initial state in our transition is not the ground state, there will be a thermal factor that will cancel out the transition rate at $T = 0$.

In order to have transitions from such a state, it has to be populated. Not only that. State $|1\rangle$ should also be at least partially depopulated. That is, we must have a non-zero thermal population difference between the two states involved in the resonant transition:

$$\Delta P = \frac{e^{-\beta\omega_0} - e^{-\beta(\Omega+\omega_0)}}{Z} = e^{-\beta\omega_0}\left(\frac{1-e^{-\beta\Omega}}{Z}\right); \qquad Z = \sum_i e^{-\beta\omega_i} \tag{31}$$

This difference can be zero because both states are equipopulated or because both are empty. If $\omega_0 = 0$ and we consider only two states, $|0\rangle$ and $|1\rangle$, then it is easy to see that we recover the usual statistical physics result of the thermal population of a two-level system:

$$\Delta P = \frac{1-e^{-\beta\Omega}}{1+e^{-\beta\Omega}} = \tanh\left(\frac{1}{2}\beta\Omega\right) \tag{32}$$

This treatment allows us to define an effective number of molecules that have an active part in the interaction with the cavity photons. This is because if a molecule is in its excited state due to thermal fluctuations, the radiation does not find an accessible excitation to be absorbed and therefore that molecule does not participate in the interaction. This effective number is simply given by

$$N_{\text{eff}} = N \cdot \Delta P \tag{33}$$

Let us now define the following collective operators [19]:

$$b^\dagger = \frac{1}{\sqrt{N_{\text{eff}}\bar{g}^2}} \sum_i^N g_i \tau_i^+ \tag{34}$$

$$\bar{g}^2 = \sum_i^N \frac{|g_i|^2}{N_{\text{eff}}} \tag{35}$$

$$[b, b^\dagger] = \frac{1}{N_{\text{eff}}\bar{g}^2}\sum_{i,j} g_i^* g_j [\tau_i^-, \tau_j^+] = \frac{1}{N_{\text{eff}}\bar{g}^2}\sum_i |g_i|^2 [\tau_i^-, \tau_i^+] = 1 - \frac{2}{N_{\text{eff}}\bar{g}^2}\sum_i |g_i|^2 \tau_i^+\tau_i^- \tag{36}$$

If we assume that $N_{\text{eff}} \gg 1$ and that there are few excited molecules, we can neglect the second term so that

$$[b, b^\dagger] \approx 1 \tag{37}$$

This transformation is known as Holstein-Primakoff transformation [20], which maps the spin operators onto bosonic creation/annihilation operators. Applying this transformation to Eq.(30) we obtain[2]:

$$\mathcal{H}_{\rm int} = \left[\sqrt{N_{\rm eff}}\bar{g}(b+b^\dagger) + \sum_i \Lambda_i \tau_i^+ \tau_i^-\right](a+a^\dagger) \tag{38}$$

The second term can be neglected if $N_{\rm eff} \gg 1$. The reason is that the non-diagonal terms scale with the root of this effective number of molecules while the diagonal ones do not:

$$b^\dagger b = \frac{1}{N_{\rm eff}\bar{g}^2}\sum_i |g_i|^2 \tau_i^+\tau_i^- = \sum_i \tau_i^+\tau_i^- \tag{39}$$

Hence

$$g \to \sqrt{N} g$$

$$\Lambda \to \Lambda$$

so, finally:

$$\mathcal{H}_{\rm int} = \bar{g}\sqrt{N_{\rm eff}}(b+b^\dagger)(a+a^\dagger) = g_{\rm eff}(b+b^\dagger)(a+a^\dagger) \tag{40}$$

Notice that, we have expressed the interaction as two coupled oscillators. The resulting effective coupling, $g_{\rm eff} = \bar{g}\sqrt{N_{\rm eff}}$, scales with the number of interacting molecules and with the overlap between the wave functions of the initial and final spin states via the $\mathcal{O}$ operator.

Putting all toghether, the Hamiltonian that describes our ensemble of magnetic molecules coupled to the resonator is

$$\mathcal{H} = \Omega b^\dagger b + \omega_{\rm r} a^\dagger a + g_{\rm eff}(b+b^\dagger)(a+a^\dagger) \tag{41}$$

where $\Omega$ accounts for the transition resonant frequency $\omega_{\rm r}$ is the LC frequency.

One might wonder whether this treatment is still valid when considering more than one resonance frequency in the molecule. This situation might arise, for example, if we have a hyperfine splitting (see Fig. 11) that gives rise to several transitions with similar frequencies.

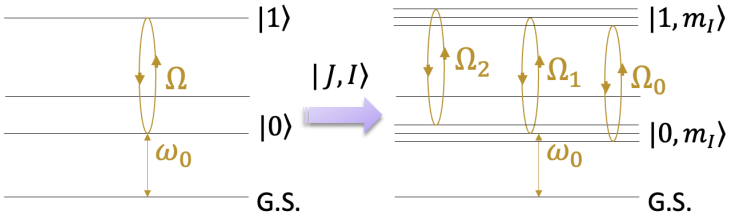


Figure 11: If we have some hyperfine splitting in our system, the energy levels could be split non-homogeneously and we could get allowed transitions that are very close in frequency. Perhaps too close to be distinguishable in an experiment.

In that cases, we project onto the states involved in the transitions of interest:

$$\mathcal{H} = \sum_{\omega_{ij}} \frac{\omega_{ij}}{2}\left[|j\rangle\langle j| - |i\rangle\langle i|\right] + \omega_{\rm r} a^\dagger a + \bar{\mathcal{O}}(a^\dagger + a) \tag{42}$$

[2]We drop from here the hats denoting the operators to gain simplicity in notation since enough emphasis was made

where

$$\bar{\mathcal{O}} = \sum_{i,j} \mathcal{O}_{i,j} \left|i\right\rangle \left\langle j\right| \tag{43}$$

is the operator mediating the transitions and the coupling between the molecule and the resonator. It is block diagonal matrix (a block per transition) Thus, it is always possible to to decompose the total Hilbert space into reduced spaces of dimension 2. To aliviate the notation, we are going to make the following change in the indexes $(i,j) \to k$, $\frac{1}{2}(\left|j\right\rangle \left\langle j\right| - \left|i\right\rangle \left\langle i\right|) \to \sigma_k^z$, so that we can now express our Hamiltonian for a single molecule in the following way

$$\mathcal{H} = \sum_k \omega_k \sigma_k^z + \omega_{\mathrm{r}} a^\dagger a + \sum_k \left[(g_k \tau_k^+ + h.c.) + \Lambda_k \tau_k^+ \tau_k^-\right](a + a^\dagger) \,. \tag{44}$$

Here, we have used the results we had obtained in Eq.(29). If we consider, again an ensemble of $N$ molecules, the Hamiltonian can be written as:

$$\mathcal{H}_{\mathrm{E}} = \omega_{\mathrm{r}} a^\dagger a + \sum_{n=1}^{N} \sum_k \left[\omega_{k,i} \sigma_{k,i}^z + \left[(g_{k,i} \tau_{k,i}^+ + h.c.) + \Lambda_{k,i} \tau_{k,i}^+ \tau_{k,i}^-\right](a + a^\dagger)\right] \tag{45}$$

Finally, we can apply the Holstein-Primakoff transformation for each spin subspace, defining bosonic operators for each transition. Within the same approximations done in the case of a single transition, we arrive to

$$\mathcal{H}_{\mathrm{E}} = \omega_{\mathrm{r}} a^\dagger a + \sum_k \left[\Omega_k b_k^\dagger b_k + g_{\mathrm{eff},k}(b_k + b_k^\dagger)(a + a^\dagger)\right] \tag{46}$$

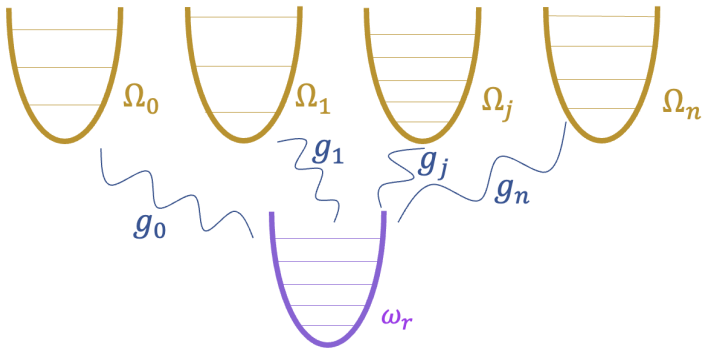


Figure 12: If we consider a set of transitions with resonant frequency close to the resonator's that are not linked between them, we can consider it as a set of uncoupled harmonic oscillators that do couple in a differentiated manner to the electromagnetic mode.

the coupling between the resonator and the corresponding spin transition is effective when the frequencies are coincident in a range determined by the photon decay rate $\kappa$. If the difference between the $\Omega_k$ is smaller than this parameter, a broadening of the resonant line occurs. On the other hand, if the difference is larger and the coupling is strong enough for each transition, the different absorption lines are resolved. We discuss all this bellow.

### 3.2 Transmission and strong coupling regime

The transmission we measure in the laboratory can be characterized through linear response theory and with an input-output type formalism. First, we characterize the input signal with

the following driving Hamiltonian that describes an oscillating signal whose amplitude we can relate to the dissipative factor of the resonator (the signal flows through the transmission line so that if there is no coupling between it and the resonator, described by the $\kappa$ parameter, the input signal will not be detected by the resonator) and it will have a driving frequency $\omega$:

$$\mathcal{H}_{\rm d} = \alpha\kappa(e^{i\omega t} + e^{-i\omega t})(a + a^\dagger) \tag{47}$$

On the other hand, the transmission is nothing but the LC resonator response, $\chi_{aa}$ to this driving. Especifically [21],

$$t(\omega) = 1 - i2\pi g(\omega)\chi_{aa}(\omega) \tag{48}$$

Here $\chi_{aa}$ means the response of operator $a$ when driving through $a$ (as in Eq. (47)) This response can be obtained computing the $\langle a\rangle$ with the help of a driven Gorini-Kossakowski-Sudarshan-Lindblad equation, or quantum master equation [22]. This master equation contains two dissipative terms: one for the intrinsic sample dissipation $\gamma$ and another one for the decay and leakage of the cavity photons $\kappa$:

$$\frac{d\rho}{dt} = -i[\mathcal{H}_T, \rho] + \sum_k \gamma_k \left( b_k \rho b_k^\dagger - \frac{1}{2}\{b_k^\dagger b_k, \rho\} \right) + \kappa \left( a\rho a^\dagger - \frac{1}{2}\{a^\dagger a, \rho\} \right) \tag{49}$$

In principle, the spin decoherence may depend on the transition considered, but for simplicity we will assume that this parameter is the same for all of them, $\gamma_k = \gamma$.

Any observable can be computed [23]

$$\frac{d}{dt}\langle\theta\rangle = +i\langle[\mathcal{H}_T, \theta]\rangle + \gamma\left\langle \mathcal{D}_\theta^\dagger[b]\right\rangle + \kappa\left\langle \mathcal{D}_\theta^\dagger[a]\right\rangle \tag{50}$$

where $\left\langle \mathcal{D}_\theta^\dagger[A]\right\rangle = \langle A^\dagger\theta A\rangle - \frac{1}{2}\langle\{A^\dagger A, \theta\}\rangle$. Using the Rotating Wave Approximation (RWA) the dynamics for the expected values of these operators is given by the following equations

$$\frac{d}{dt}\langle a\rangle = i\left(\omega - \omega_{\rm r} + i\frac{\kappa}{2}\right)\langle a\rangle - i\sum_k g_{{\rm eff},k}\langle b_k\rangle - i\alpha\kappa \tag{51}$$

$$\frac{d}{dt}\langle b_k\rangle = i\left(\omega - \Omega_k + i\frac{\gamma}{2}\right)\langle b_k\rangle - ig_{{\rm eff},k}\langle a\rangle \tag{52}$$

that can be solved:

$$\langle a\rangle = \frac{\alpha\kappa}{(\omega - \omega_{\rm r} + i\kappa/2) - \sum_k \frac{g_{{\rm eff},k}^2}{(\omega - \Omega_k + i\gamma/2)}} \tag{53}$$

Thus, the transmission reads [cf. Eq.(48)]

$$t(\omega) = 1 - \frac{i\kappa}{(\omega - \omega_{\rm r} + i\kappa/2) - \sum_k \frac{g_{{\rm eff},k}^2}{(\omega - \Omega_k + i\gamma/2)}} \tag{54}$$

The shape of this transmission curve is that of a Lorentzian that may present one or two absorption peaks depending on the coupling regime in which we find ourselves. If the coupling between the sample and the electromagnetic mode is weak, only one peak is resolved, corresponding to the resonance condition $\omega = \Omega_k = \omega_{\rm r}$. If the coupling is strong enough two peaks located at $\omega \approx \omega_{\rm r} \pm g_{\rm eff}$ are obtained (see Fig. 13). Between these two cases there is a fundamental difference. In the first case, the energy absorbed from the input radiation generates an excitation at either the sample or the cavity. However, if light and matter interact sufficiently intensely, the

degeneracy is broken and the light matter hibridizes in the so-called polaritons, superpositions of spin and cavity excitations. Similarly to bonding and anti-bonding states, symmetric and antisymmetric superpositions of light and matter excitations have a different energy, thus leading to two well-resolved resonances in the transmission spectrum.

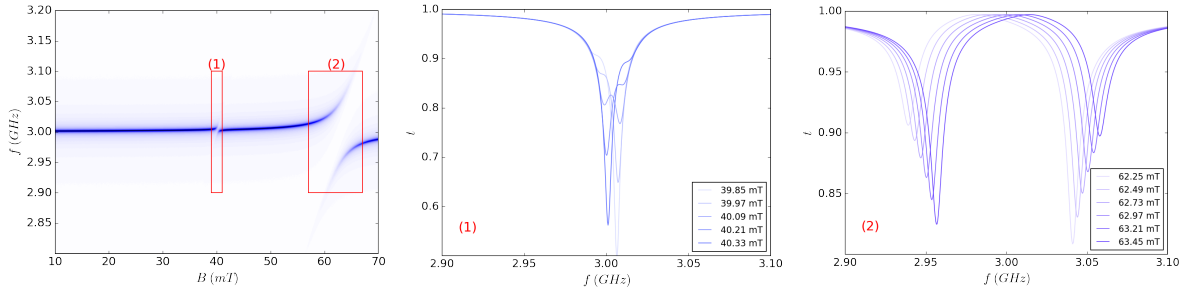


Figure 13: Simulation of Eq.(54) in a fictitious scenario where the cavity has a resonant frequency of 3 GHz and the sample has two resonant frequencies at different fields and with different couplings. The cuts denoted as (1) and (2) show the evolution of the Lorentzians for different fields. If the coupling is not very strong, situation (1), it can happen that although we have a double peak situation, the separation between them is not enough to experimentally resolve it. We see that if the coupling were, smaller than the dissipation constant, the two peaks would converge into one. However, when the coupling is strong enough, situation (2), the two peaks are well differentiated, the separation between them being proportional to the coupling of the sample to the cavity, which is known as the Rabi frequency.

What determines the boundary between strong and weak coupling? In order to distinguish the two peaks we have to obtain a coupling that is larger than the dissipative terms, i.e., larger than $\kappa$ and $\gamma$. This is experimentally demanding, since the spin decoherence term can be of the order of a few MHz and the typical single spin coupling is of the order of Hz. To reduce this difference we try to involve as many spins as possible to increase the coupling [cf. Eq.(40)]. However, the more concentrated our sample is, the higher the intensity of the dipole interactions between the molecules, which ultimately dominates and determines the decoherence time $T_2$, thus $\gamma \approx T_2^{-1}$ [24]. To mitigate this effect, we try to design diluted samples, so that for a concentration of the order of 10% we can obtain decoherence times of the order of or greater than 1 $\mu$s [25], with which we lose spins to gain in resolution and control time. Molecular design provides a direct way to dilute the sample by means of replacing Mn(II) with e.g. Zn(II) that is chemically equivalent but diamagnetic.

We must therefore try to design our circuits efficiently and optimally so that the electromagnetic modes are sufficiently intense and, at the same time, spread over a volume that contains as many spins as possible with the maximum intensity. For this reason, we work with LC circuits such as those described at the beginning of this chapter. The next section provides examples of LER designs which constitute the state of the art in their technology. Our goal here is to estimate, under realistic conditions the strength of the electric and magnetic couplings.

### 3.3 Designs and simulations

The LER circuit consists of an interdigitated capacitor and an inductor coil, as shown in Fig. 14. This type of circuits present a number of important advantages over the more "popular"

resonators based on coplanar transmission waveguides. First, the resonator impedance does not affect the transmission through the readout line. This means that one has a virtually unlimited freedom for designing the properties of the inductor and the capacitor, with the sole limitation of the desired resonance frequency. Second, the electric and magnetic photon fields are spatially separated from each other, thus offering an ideal platform to explore and compare the coupling to each of them. Details on the distribution of the fields in each zone can be also checked in Fig. 14. This type of circuits as well as other designs are manufactured by our collaborators at the Centro de Astrobiología de Madrid (CSIC-INTA).

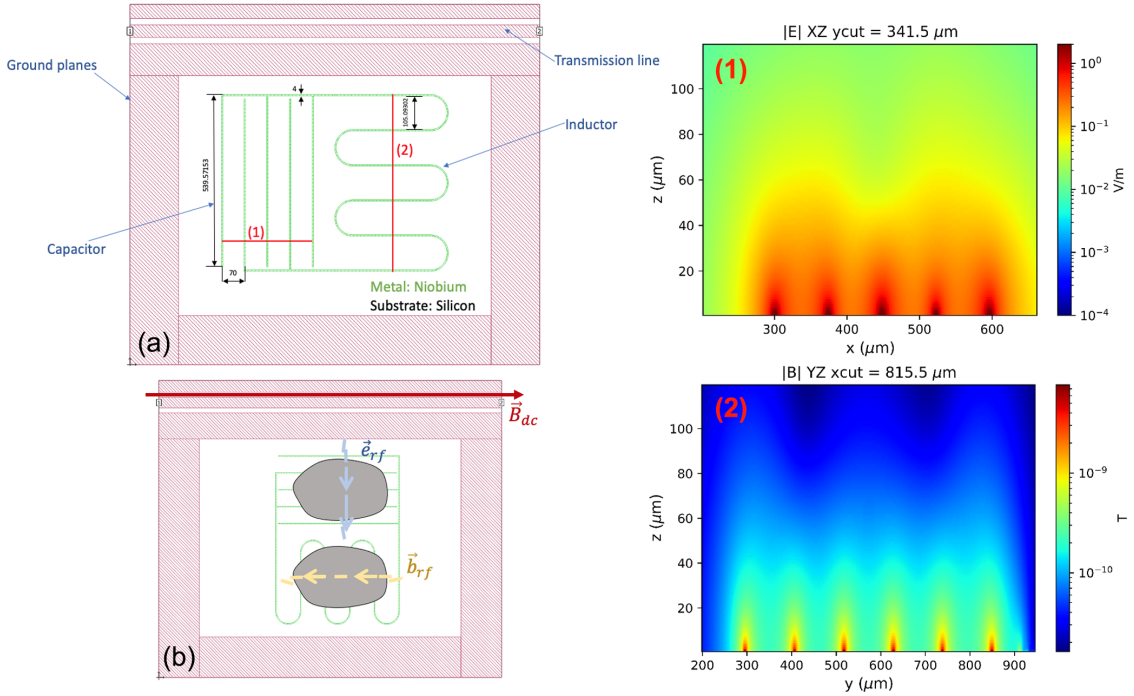


Figure 14: Design of the resonator circuit. (a) In green is the Niobium superconducting line that makes up the LC circuit. On the left, the area marked as (1), corresponds to an interdigital capacitor, which allows us to obtain electric field lines not only between plates, but also out of the plane, as can be seen in the map in the top-right corner labelled as (1). The right hand panel labelled as (2) corresponds to the inductor coil through which the flow of current generates a magnetic field that surrounds the coil. The corresponding magnetic field map is in the bottom-right corner, labelled as (2). (b) Geometrical display of the LER circuit with respect to the transmission line. We can place one sample on top of the capacitor or the inductor depending on the type of coupling we seek.

The resonant frequency of the resonator found for these specifications corresponds to 10.56 GHz, while the quality factor, $Q = f_{\text{res}}/\kappa$, is of the order of $2 \times 10^4$, giving a photon decay rate, $\kappa$, of about 500 kHz. On the other hand, using the density of our sample is $2.1 \times 10^9$ spins/$\mu$m$^3$, and the dimensions of the circuit, we can estimate the number of spins that interact with the cavity mode. For a concentration of 10%, we estimate a decoherence factor, $\gamma$, of about 1 MHz or less [24]. With all these parameters and the theory developed in the previous sections, we proceed to simulate the transmission with Eq.(54). We do it in two circunstances, coupling the sample to either the inductor (i.e. to the magnetic field) or the capacitor (electric field). The results of these simulations are shown in Fig. 15, where we have chosen a temperature of 10

mK, a sample volume of $400 \times 200 \times 40$ $\mu$m$^3$ and two orientations of the symmetry axis of the molecule: parallel and perpendicular to the DC magnetic field, respectively.

Wit the field range chosen we are able to resolve the 6 lines corresponding to the hyperfine splitting between the two multiplets involved in the transition, with the exception of Fig. 15a, where two of the resonance lines are located in a larger field. We can conclude that there is a large coupling to both the magnetic field (thanks to its 5/2 spin) and to the electric field. While the most favourable case for strong magnetic coupling is the one where the anisotropy axis is perpendicular to the DC magnetic field (Fig. 15b), the electric coupling is similar in both orientations.

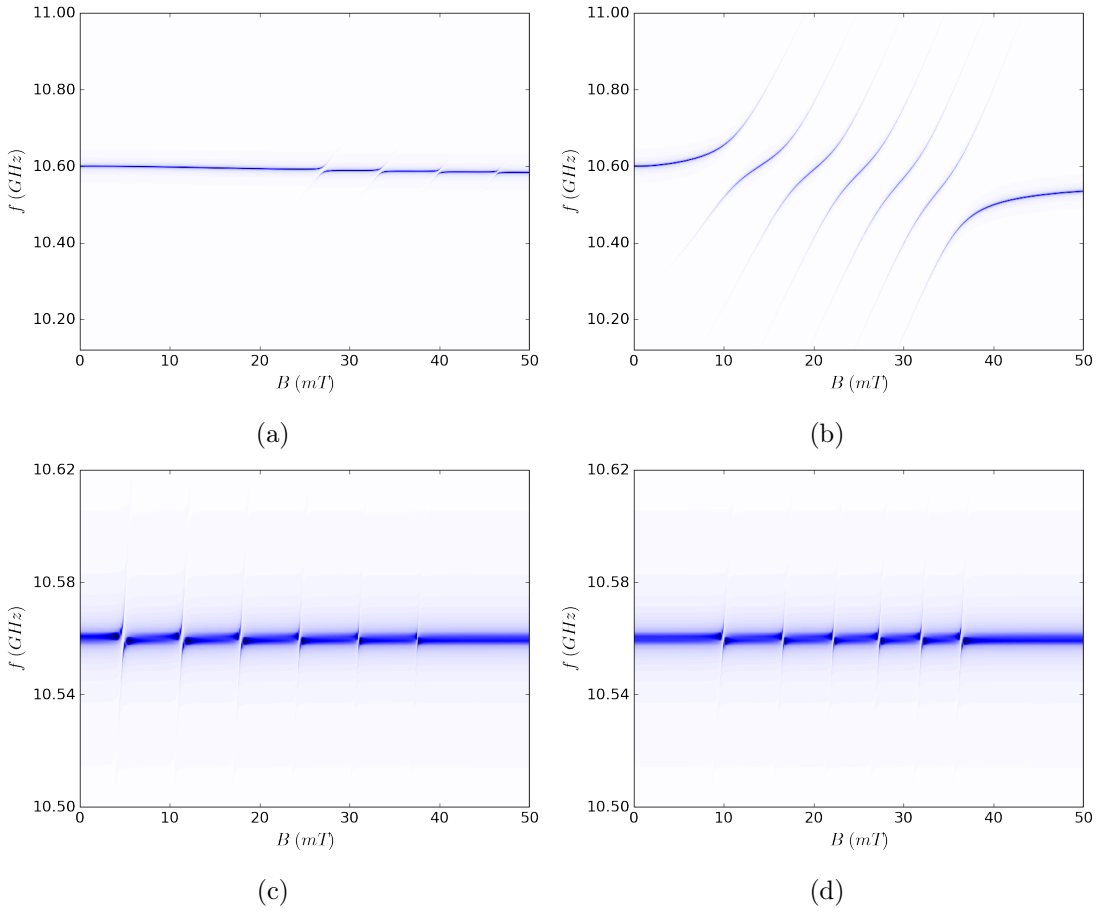


Figure 15: Transmission spectra obtained through Eq.(54) for both electrical coupling (plots (c) and (d)) and magnetic coupling (plots (a) and (b)). The left column (plots (a) and (c)) represents a scenario where the symmetry axis of the sample is parallel to the applied DC magnetic field [cf. Fig. 14], while the right column represents a situation where the symmetry axis is perpendicular to the field. The simulations were made assuming a temperature of 10 mK. As can be seen, we obtain a strong coupling situation in all scenarios, the coupling through the magnetic field being superior.

Although the coupling strength in the magnetic case is still larger than that in the electric case, the electric coupling is large enough to be detectable in an experiment. Specifically, the Rabi frequencies obtained in the electric case (see Fig. 16), are 11.3 MHz for the case where the crystal symmetry axis and the DC magnetic field are parallel and 7 MHz for the case where they are perpendicular, which means an operating time of about 10 $\mu$s.

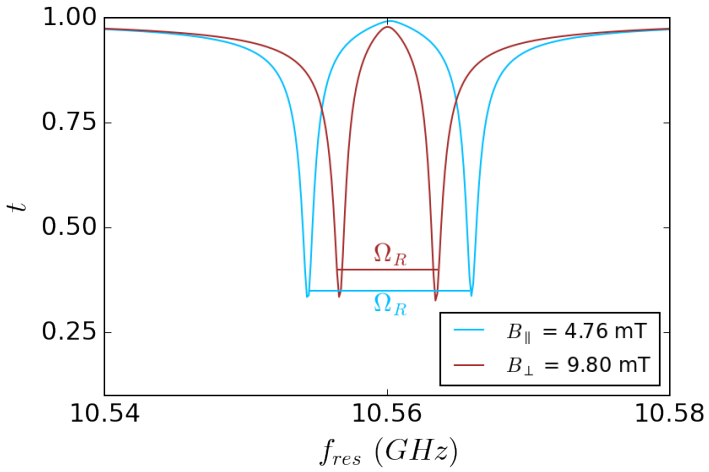


Figure 16: Maximum Rabi frequencies obtained for electrical coupling. Each curve is a cut-off to the field shown in the legend in figures 15c and 15d. The blue line corresponds to the DC magnetic field situation parallel to the anisotropy axis (Fig. 15c) while the brown line corresponds to the field perpendicular to the axis (Fig. 15c). The Rabi frequencies obtained for each case are, respectively, $\Omega_{R,\parallel} = 11.3$ MHz and $\Omega_{R,\perp} = 7$ MHz

.

## Conclusions & outlook

From this Master's thesis we can conclude that

- Spins can be controlled by electric fields both to tune their resonance frequencies and to coherently manipulate their states.
- Magnetic molecules, like $Mn(Me_6tren)Cl\_ClO_4$, show a remarkably high magnetoelectric effect thanks to the design of the metal coordination that modulates this effect through the combined action of the crystal field and the spin-orbit coupling.
- This effect gives rise to sizeable spin-photon couplings for suitable experimental conditions (crystal orientation and magnetic field values) and properly designed superconducting resonators.
- It seems that reaching a strong coupling of molecular spins to the electric field of cavity photons can be achieved.
- Besides, this effect will be enhanced at very small size scales. This might provide a promising route to wiring up molecular spin qubits and a scalable architecture.

Although this work has focused on the study of $Mn(Me_6tren)Cl\_ClO_4$, we do not rule out exploring other options such as $TbPc_2$, which we discussed in section 1, as well as any other molecule that has suitable characteristics for electrical control. Furthermore, we are carrying out experiments at QMAD to characterise synthesised crystals of $Mn(Me_6tren)Cl\_ClO_4$ to check all of its properties through thermodynamical measurements and we expect in the near future to manufacture the resonators presented in this work in order to carry out transmission experiments and check the magnetoelectric effect described.

## References


1. Arute, F. *et al.* Quantum supremacy using a programmable superconducting processor. *Nature* **574,** 505–510 (2019).
2. Loss, D. & DiVincenzo, D. P. Quantum computation with quantum dots. *Physical Review A* **57,** 120 (1998).
3. Imamog, A. *et al.* Quantum information processing using quantum dot spins and cavity QED. *Physical review letters* **83,** 4204 (1999).
4. Bartolome, S. J., Luis, F. & Fernández, J. F. *Molecular magnets* (Springer, 2016).
5. Gimeno, I. *et al.* Broad-band spectroscopy of a vanadyl porphyrin: a model electronuclear spin qudit. *Chemical Science* **12,** 5621–5630 (2021).
6. Jenkins, M. D. *Coupling quantum circuits to magnetic molecular qubits* (2015). arXiv: 1507.03579 [cond-mat.mtrl-sci].
7. Ballhausen, C. J. *Introduction to ligand field theory* tech. rep. (McGraw-Hill, 1962).
8. Coey, J. M. *Magnetism and magnetic materials* (Cambridge university press, 2010).
9. White, R. M., White, R. M. & Bayne, B. *Quantum theory of magnetism* (Springer, 1983).
10. Abragam, A. & Bleaney, B. *Electron paramagnetic resonance of transition ions* (OUP Oxford, 2012).
11. Trif, M., Troiani, F., Stepanenko, D. & Loss, D. Spin-electric coupling in molecular magnets. *Physical review letters* **101,** 217201 (2008).
12. Trif, M., Troiani, F., Stepanenko, D. & Loss, D. Spin electric effects in molecular antiferromagnets. *Physical Review B* **82,** 045429 (2010).
13. Boudalis, A., Robert, J. & Turek, P. First Demonstration of Magnetoelectric Coupling in a Polynuclear Molecular Nanomagnet: Single-Crystal EPR Studies of [Fe3O (O2CPh) 6 (py) 3] ClO4 py under Static Electric Fields. *Chemistry-A European Journal* **24,** 14896–14900 (2018).
14. Petersson, K. D. *et al.* Circuit quantum electrodynamics with a spin qubit. *Nature* **490,** 380–383 (2012).
15. Nowack, K. C., Koppens, F., Nazarov, Y. V. & Vandersypen, L. Coherent control of a single electron spin with electric fields. *Science* **318,** 1430–1433 (2007).
16. Fittipaldi, M. *et al.* Electric field modulation of magnetic exchange in molecular helices. *Nature materials* **18,** 329–334 (2019).
17. Thiele, S. *et al.* Electrically driven nuclear spin resonance in single-molecule magnets. *Science* **344,** 1135–1138 (2014).
18. George, R. E., Edwards, J. P. & Ardavan, A. Coherent spin control by electrical manipulation of the magnetic anisotropy. *Physical review letters* **110,** 027601 (2013).
19. Hümmer, T., Reuther, G. M., Hänggi, P. & Zueco, D. Nonequilibrium phases in hybrid arrays with flux qubits and nitrogen-vacancy centers. *Physical Review A* **85,** 052320 (2012).
20. Holstein, T. & Primakoff, H. Field Dependence of the Intrinsic Domain Magnetization of a Ferromagnet. *Phys. Rev.* **58,** 1098–1113. https://link.aps.org/doi/10.1103/PhysRev.58.1098 (12 Dec. 1940).

21. Sánchez-Burillo, E. *One-dimensional few-photon scattering: Numerical and analytical techniques* ().

22. Breuer, H.-P., Petruccione, F., *et al. The theory of open quantum systems* (Oxford University Press on Demand, 2002).

23. Roca Jerat, S., Zueco Láinez, D. & Luis Vitalla, F. Generación de estados de espín "squeezed" en materiales híbridos. https://deposita.unizar.es/record/54201?ln=es (2020).

24. Morello, A., Stamp, P. & Tupitsyn, I. S. Pairwise decoherence in coupled spin qubit networks. *Physical review letters* **97,** 207206 (2006).

25. Ardavan, A. *et al.* Will spin-relaxation times in molecular magnets permit quantum information processing? *Physical review letters* **98,** 057201 (2007).